



Cite this: *New J. Chem.*, 2021, **45**, 4246

A PdCu nanoalloy catalyst for preferential CO oxidation in the presence of hydrogen†

Rohini Khobragade,^{ib}^a Pranali Dahake,^a Nitin Labhsetwar^{ib}^a and Govindachetty Saravanan^{ib}^{*b}

Catalytic oxidation of carbon monoxide (CO) is one of the essential steps for several environment- and energy-related applications. Here, we report the synthesis of alloy PdCu nanoparticles supported on an Al₂O₃ support as a catalyst for effective removal of CO from H₂-rich flue gases. The alloy phase between Pd and Cu was formed by deposition of organometallic Pd- and Cu-precursors on the Al₂O₃ support followed by thermal reduction under H₂. The alloy PdCu nanoparticles (average size: 30 nm) are in a spherical shape and they are distributed in the range between 10 and 80 nm. The alloy PdCu catalyst showed improved CO oxidation performance both in the presence and absence of H₂ compared to that of the reference Pd catalyst. It is also inferred that the alloy PdCu catalyst showed an onset temperature (*T*_o) of 50 °C in the presence of H₂ compared to that of CO oxidation in the absence of H₂ (*T*_o = 100 °C). In addition, the alloy PdCu catalyst showed selective CO oxidation performance below a temperature range of 300 °C. Therefore, the formation of the Pd-based alloy structures may have potential as the preferential CO oxidation catalyst for the catalytic removal of CO from various flue gases.

Received 1st January 2021,
 Accepted 28th January 2021

DOI: 10.1039/d1nj00005e

rsc.li/njc

Introduction

Removal of toxic carbon monoxide (CO) from various flue gases using catalysts, for instance automobile exhaust tailpipe emissions that contain significant amounts of CO, partial combustion of biomasses from unorganized sectors, H₂-rich flue gases as a result of reforming followed by water–gas shift reactions, *etc.* is taking wide attention due to not only its toxic behavior but also the need of continuous power generation for decentralized applications in particular transportation, telecom tower, hospital and military applications, *etc.*^{1–6} The flash point of CO (*i.e.*, a temperature that oxidizes CO completely) is generally above 600 °C in the absence of any catalysts, which is a cost- as well as energy-intensive processes. On the other hand, it can be reduced significantly upon the use of catalysts under the given CO oxidation conditions due to their proven surface characteristics. The removal of CO from the H₂-rich gases *via* preferential CO oxidation (CO-PROX) using the catalysts is one of the vital steps to generate cleaner energy

continuously through polymer electrolyte membrane fuel cells with minimum greenhouse gas emissions.^{7–10}

Transition metal-based catalysts in the form of metals, mixed metals, oxides, mixed oxides, spinels, perovskites, *etc.* are considered for the removal of CO from the flue gases.^{11–13} However, the performance for instances catalytic activity at a relatively low onset temperature, long-term catalytic performance, *etc.*, needs to be improved further than that of the currently existing catalysts. Platinum group metals (PGM) showed much better catalytic performance compared to that of the oxide-based catalysts due to their surface characteristics, however, their cost and scarce minerals pose persistent challenges to their use as catalysts for the target applications at a larger scale.¹⁴ In addition, the stability of the existing catalyst structures (metals or metal oxides) under the severe CO oxidation conditions is another serious concern among others, which has to be improved significantly. Therefore, catalysts with improved catalytic performance and ameliorated stability at a lower cost have to be developed for the catalytic removal of CO from flue gases. This can be readily achieved by the development of PGM-based intermetallic- or alloy-catalyst structures with minimum possible amounts of PGM. Alteration in the d-band centers and electronic structures, bi-functional characteristics, *etc.* are the major attributes to the improved performance of the intermetallic or alloy catalysts compared to that of their individual counterparts.^{15–17} The ever-developed alloy or intermetallic catalysts show improved performance along with ameliorated stability compared to that of

^a Energy and Resource Management Division, CSIR-National Environmental Engineering Research Institute (CSIR-NEERI), Nehru Marg, Nagpur 440 020, India

^b Chennai Zonal Centre, CSIR-National Environmental Engineering Research Institute (CSIR-NEERI), CSIR-Madras Complex, Taramani, Chennai 600 113, India. E-mail: g_saravanan@neeri.res.in

† Electronic supplementary information (ESI) available. See DOI: 10.1039/d1nj00005e

their individual counterparts at the same or less-PGM loading.^{18–22} Although Pt-based alloy or intermetallic catalysts have shown superior CO-PROX performance compared with the reference Pt catalysts, investigations are still required to find an alternative to the state-of-the-art Pt catalyst (*e.g.*, Pd and its alloys) for most of the catalysis reactions due to its cost and scarce minerals.^{14,23–25}

Pd-based intermetallic or alloy catalysts were developed for various catalytic applications. Pd₃Cu alloy nanocrystals were synthesized through a polyol reduction without any shape directing agents that showed catalytic formic acid oxidation performance for direct fuel cells.²⁶ An intermetallic PdCu catalyst supported on ZnAl₂O₄ was developed for the selective production of H₂ through a steam reforming reaction in methanol.²⁷ It was observed that the intermetallic phase between Pd and Cu was formed through a spillover mechanism.²⁸ Pd- or Rh-based intermetallic catalysts were prepared for hydrogenation of *p*-nitrostyrene and cyclohexane derivatives or methanol as the source of H₂.²⁹ It was observed that the intermetallic PdPb catalyst offered a better chemo-selective hydrogenation performance due to the higher electronegativity of Pb among other elements used for the synthesis of Pd-based intermetallics. Intermetallic PdGa compounds were developed for the selective, partial-hydrogenation reaction for acetylene. It was observed that the electronic structures at the Fermi level of Pd were modified in the PdGa intermetallics due to the presence of Ga atoms around Pd.³⁰ Bimetallic PdCu catalysts were developed for the synthesis of methanol through hydrogenation of CO₂. It was observed that the PdCu bimetallic catalyst possesses a synergistic effect for the hydrogenation of CO₂.³¹ Despite several advantages of the Pd-based intermetallic or alloy catalysts, these catalysts haven't been tested for the removal of CO in the presence of H₂, which is attempted in this study, and is an important step for the generation of continuous power with improved fuel efficiency through fuel cells for decentralized applications.

In this work, Al₂O₃ supported alloy PdCu nanoparticles as a catalyst were realized using an impregnation method followed by thermal reduction under a H₂ environment for the catalytic removal of CO *via* an oxidation reaction both in the presence (CO-PROX) and absence of H₂ (Fig. 1). XRD- and XPS-analyses

were used to examine the formation of alloy phases between Pd and Cu. HR-TEM analysis was used to observe the morphology and particle size distribution of the catalysts. ICP-OES was used to estimate the concentration of Pd and Cu present in the catalysts. Similarly, Al₂O₃ supported Pd nanoparticles were also synthesized and characterized as a reference catalyst to the alloy PdCu catalyst. The catalytic activity of the alloy PdCu and Pd catalysts was examined under CO and CO-PROX conditions.

Experimental

Materials

Organometallic salts of palladium(II) 2,4-pentanedionate (C₁₀H₁₄O₄Pd; Pd assay = 34.7%) and copper(II) 2,4-pentanedionate (C₁₀H₁₄O₄Cu, 98%) were purchased from Alfa Aesar. Nano γ -Al₂O₃ powder was procured from SRL Pvt. Ltd. Analytical reagent grade HCl (37%) and HNO₃ (69%) and HPLC grade methanol were purchased from Merck Ltd. O₂ (99.99%) and He (99.998%) and the physical gaseous mixture of CO (2%) and H₂ (70%) balanced with He, H₂ (5%) gas as a reducing agent balanced with N₂, and CO (5%) balanced with He were supplied by Alchemie gases and chemicals Pvt. Ltd.

Synthesis of Pd and alloy PdCu nanoparticles on Al₂O₃

Pd- or alloy PdCu-nanoparticles on the Al₂O₃ support as the catalysts were prepared by a wet-impregnation method. 5 wt% of metallic Pd-loading was maintained on the Al₂O₃ support for both the catalysts. The organometallic salts of Pd (0.1433 g, 0.4697 mmol) and Cu (0.0689 g, 0.2632 mmol) were dissolved in methanol (50 ml) at room temperature. Nano Al₂O₃ powder was mixed with the methanolic solution of organometallic Pd- and Cu-salts followed by stirring for 6 h. The composite solutions were heated at 70 °C in order to deposit the organometallic salts on the Al₂O₃ powder. The resultant product was ground for 15 min using a mortar and pestle followed by heating at 800 °C under a H₂ atmosphere for 8 h. Pd nanoparticle supported Al₂O₃ as the reference catalyst was prepared similarly, however, without the Cu-salts. It should be noted that all the experimental conditions were the same to prepare these catalysts.

Characterization

pXRD analysis was performed by scanning (2θ range) of the Pd- and alloy PdCu-catalysts between 10 and 90° in order to examine the formation of alloy phase between metallic Pd and Cu. CuK α radiation ($\lambda = 0.15418$ nm) was generated from a Cu source using an X-ray diffractometer (Miniflex II-DD34863). The shape, size and distributions of the Pd- and alloy PdCu-nanoparticles on the Al₂O₃ support were observed at an acceleration voltage of 200 kV by HR-TEM analysis (JEM-2100F). The Pd and alloy PdCu catalysts were sonicated in ethanol for 10 min followed by recovering them on a Cu grid (200 mesh) as per standard TEM sample preparation. The concentration of Pd and Cu present in the catalysts was quantified by ICP-OES (Thermo Fischer, iCAP 6300 DUO). An aliquot amount of the Pd

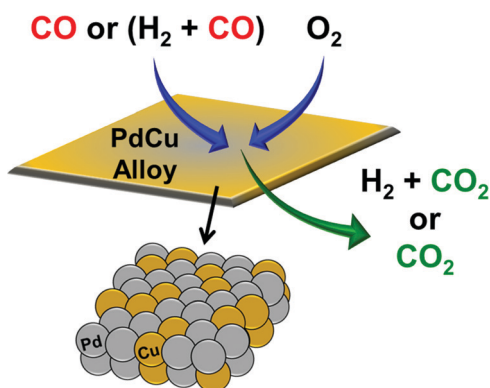


Fig. 1 Pictorial representation of catalytic CO oxidation in the presence and absence of H₂ on the surface of a PdCu alloy system.

or alloy PdCu catalysts (10 mg) was carefully digested in aquaregia (1:3, HNO₃ and HCl) and their corresponding dilutions were made as per standard ICP protocol. The oxidation states of Pd and Cu of the catalysts were examined by XPS analysis (JEOL, JPS 9010MC) using Al K α radiation. The narrow- and survey-scans of the catalysts were recorded at the pass energies of 40 and 160 eV, respectively. Conductive carbon was mixed with the catalysts using a mortar and pestle in order to exclude the possible charging effect due to the insulator behaviour of the Al₂O₃ support during the XPS analysis. The composition of the PdCu catalyst was quantified further by integration of the corresponding photoemission peaks.

Catalytic activity

The CO oxidation reaction of the catalysts under CO and CO-PROX conditions was examined using a fixed bed catalytic reactor that contains adequate mass flow controllers for various set gases, a temperature programmable furnace, gas chromatography with a thermal conductivity detector, *etc.* 50 mg of the Pd or alloy PdCu catalysts were placed between the quartz wool inside the quartz reactor that is fixed in the bore of the furnace. Stoichiometric CO or H₂/CO and O₂ gases were subjected on the catalysts to evaluate their catalytic CO oxidation performance. Feed gases (flow rate: 50 ml min⁻¹) containing CO (2%) and O₂ (5%) for the CO oxidation and CO (2%) and H₂ (70%) balanced by He and O₂ (1%) for the CO-PROX oxidation were subjected on the catalysts to examine their performance. Both the catalysts were pre-treated at 200 or 500 °C for 1 h under the feed gas environment prior to the catalytic CO oxidation. After the pre-treatment, the catalysts were heated from ambient temperature to 300 or 500 °C in the presence of the desired gaseous compositions. The concentration of the feed- and outlet-gases after the catalysis reaction was analyzed using a carboxane column (Supelco Analytical) at every set temperature. All of the catalytic evaluations of the catalysts were performed at least three times and the obtained values were averaged to examine their catalytic performance.

Results and discussion

Catalyst characterization

Fig. 2 shows the XRD patterns of the as-synthesized Al₂O₃ supported Pd nanoparticles (hereafter denoted as Pd/Al₂O₃) and the alloy PdCu nanoparticles (hereafter denoted as PdCu/Al₂O₃). The XRD pattern of Pd/Al₂O₃ showed characteristic peaks at 40.0°, 46.6°, 68.0°, 82.1° and 86.5° for the planes of (111), (200), (220), (311), and (222), respectively (JCPDS #: 01-088-2335) (FCC-type structure, *Fm* $\bar{3}$ *m*, *a* = 0.38 nm). The XRD pattern of the PdCu/Al₂O₃ also showed similar characteristic peaks, however, shifted to higher angles and observed at 40.6°, 47.3°, 69.1°, 83.4° and 88.0°, corresponding again to FCC-type structure (*Fm* $\bar{3}$ *m*, *a* = 0.37 nm) due to the formation of alloy phase between Pd and Cu. It should be noted that this catalyst showed no other characteristic diffraction peaks corresponding to metallic

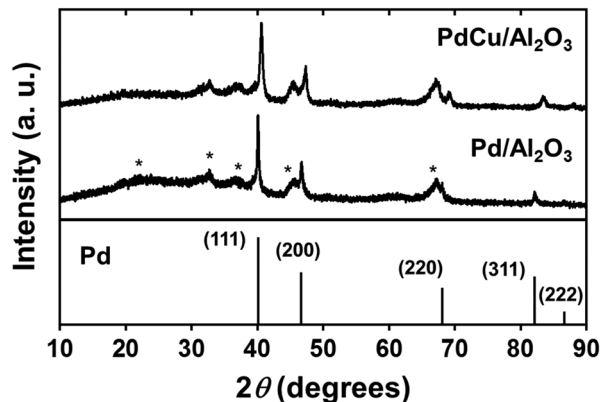


Fig. 2 pXRD patterns for Pd/Al₂O₃ and alloy PdCu/Al₂O₃. Simulated lines for Pd are shown for reference. The XRD diffraction peaks for the Al₂O₃ support are shown as asterisks.

Cu or oxides of Cu (CuO and Cu₂O) (Fig. S1, ESI†). Although the calculated total metal loading (Pd and/or Cu) is relatively low (~5–6.7 wt%) in the synthesized catalysts (see ICP-results), the characteristic diffraction peaks were very clearly observed due to the adopted synthesis conditions that facilitate ordered alloy structures between Pd and Cu, where the impregnated Pd- and Cu-precursors were heated at 800 °C under a H₂ atmosphere. The observed results are consistent with earlier studies.³² It should be noted that both the catalysts showed the characteristic diffraction peaks for the Al₂O₃ support in the XRD patterns marked as asterisks.

Pd nanoparticles of the Pd/Al₂O₃ catalyst are in a spherical shape that is finely dispersed on the support as shown in Fig. 3a. The average particle size of the Pd nanoparticles is 30 nm and their size is in the range between 15 and 40 nm (Fig. 3b). Similarly, the alloy PdCu nanoparticles are also dispersed on the Al₂O₃ support and are in a spherical shape (Fig. 3c), however, their size is slightly in a higher range compared to that of the Pd nanoparticles, which are observed between 10 and 80 nm (Fig. 3d). It should be noted that the average particle size of the alloy PdCu is, however, virtually the same as that of the Pd nanoparticles dispersed on the Al₂O₃ support, observed at 30 nm. These results inferred that the particle size range of Pd nanoparticles increased when Cu-salts were used for the synthesis of the alloy PdCu system. The observed results are consistent with our previous results, where the particle size of intermetallic PtCu nanoparticles increased with increase of the Cu-amounts during the synthesis.³³ The surface of Pd- and alloy PdCu-nanoparticles was observed further to see the facets present, which is very important to facilitate the catalysis reaction. The surface of the Pd nanoparticles is atomically ordered with a *d*-spacing value of 0.23 nm, assigned to the {111} plane (Fig. 3e). Similarly, the surface of the alloy PdCu nanoparticles is also atomically ordered and their *d*-spacing value is calculated to be 0.22 nm, assigned again to the {111} plane, which is virtually the same as that of the Pd nanoparticles (Fig. 3f). These results inferred that the surface of the Pd nanoparticles is not altered significantly upon the addition of Cu content in its lattice.

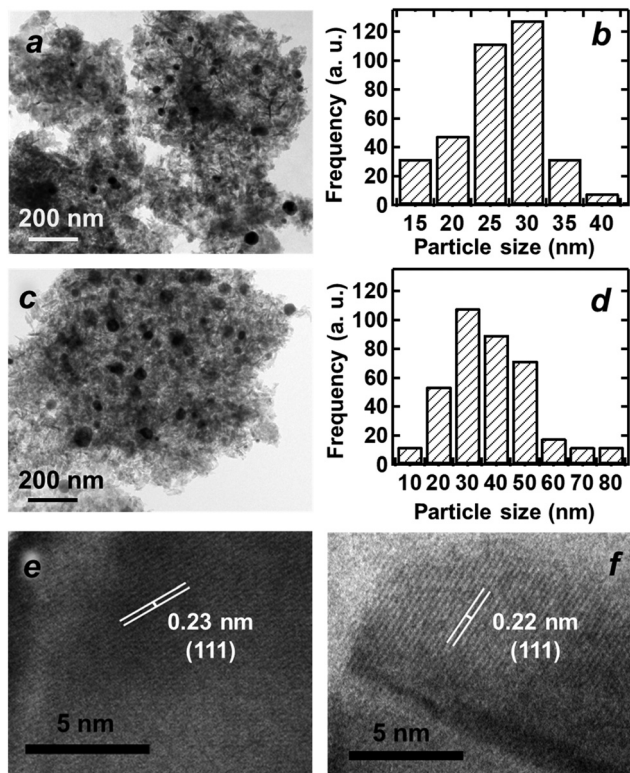


Fig. 3 TEM image of Pd/Al₂O₃ (a) and alloy PdCu/Al₂O₃ (c) and their particle size distribution is shown in the histograms (b and d). HR-TEM image of Pd/Al₂O₃ (e) and alloy PdCu/Al₂O₃ (f).

The oxidation states of Pd and Cu were examined by XPS analysis. The XPS data of the Pd and alloy PdCu catalysts in the regions of Pd 3d and Cu 2p are shown in Fig. 4. The charging effect due to the non-conductive nature of the Al₂O₃ support was eliminated by mixing of the catalysts with Vulcan carbon, where the binding energy of C 1s was observed at 284.4 eV.^{32,34} Pd/Al₂O₃ showed a characteristic doublet, spin-orbit photoemission peaks at 340.2 and 335.1 eV, corresponding to 3d_{3/2} and 3d_{5/2}, respectively, due to the presence of metallic Pd in the catalyst that is formed upon reduction of the organometallic Pd-salts under the H₂ environment at 800 °C (Fig. 4a). PdCu/Al₂O₃ also showed the characteristic doublet, spin-orbit photoemission peaks corresponding to metallic Pd, however, they are shifted to a slightly higher binding energy level by ~0.3 eV. As can be seen in more detail, the doublet photoemission peaks for Pd 3d_{3/2} and 3d_{5/2} of the alloy PdCu/Al₂O₃ catalyst were observed at 340.5 and 335.4 eV, respectively. Although metallic Pd was formed upon reduction, the observed higher binding energy shift for Pd of the alloy PdCu/Al₂O₃ catalyst is due to the formation of alloy phase with Cu, which alters slightly the electronic structure of metallic Pd in the alloy PdCu catalyst. It should be noted that the spin-orbit splitting (*d*) value was observed to be ~5.1 eV for both the catalysts, which is consistent with the reported results.³² From this result, it can be understood that the metallic Pd was formed upon reduction of the organometallic Pd-salts under a H₂ environment, which is most likely involved in the formation of alloy phase with

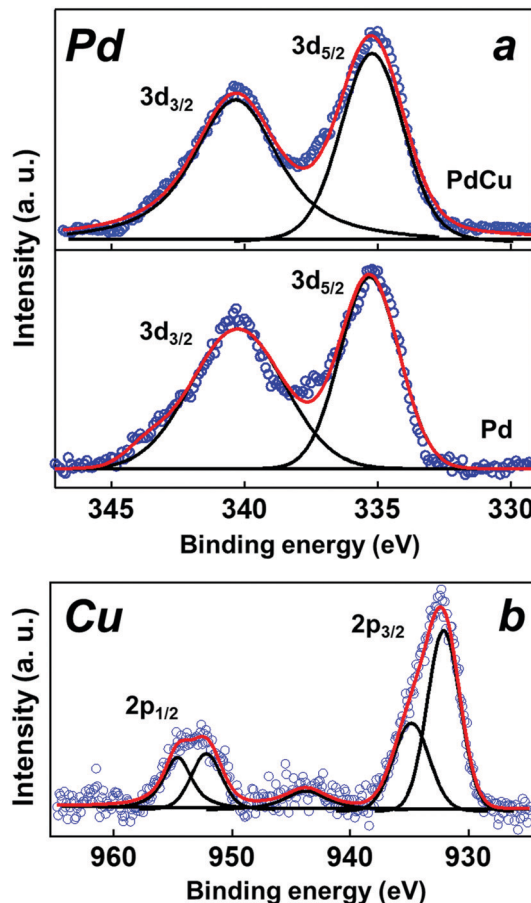


Fig. 4 X-ray photoelectron spectral profiles of Pd/Al₂O₃ and alloy PdCu/Al₂O₃ in the regions of Pd 3d (a) and Cu 2p (b).

metallic Cu formed upon reduction of the organometallic Cu-salts under a H₂ environment at 800 °C in the case of PdCu/Al₂O₃. Fig. 4b shows the XPS profile of the alloy PdCu/Al₂O₃ catalyst in the region of Cu 2p. Two clear asymmetric peaks were observed in the regions of 930–940 eV and 950–960 eV along with a broader peak at 943.8 eV, indicating that Cu exists in more than one oxidation state in the alloy PdCu catalysts. Therefore, each asymmetric peak was deconvoluted further to identify the oxidation states of Cu present in the catalysts by fitting the experimental data with the Voigt function. The Cu 2p_{3/2} peak was deconvoluted into two characteristic peaks having the binding energies of 931.9 and 934.5 eV. Similarly, a Cu 2p_{1/2} peak was deconvoluted into two characteristic peaks and observed at 952.1 and 954.6 eV. The doublet, spin-orbit photoemission peaks observed at 931.9 and 952.1 eV, correspond to metallic Cu, whereas the doublet, spin-orbit photoemission peaks observed at 934.5 and 954.6 eV correspond to CuO. It should be noted that the observed binding energies of metallic Cu are slightly lower than that of the pristine metallic Cu surface (2p_{1/2} = 932.6 eV; 2p_{3/2} = 952.6 eV)³⁵ due to the formation of alloy phase between Pd and Cu. It may be recalled that the Pd of the alloy PdCu catalyst showed a higher binding energy shift (~0.3 eV) compared with metallic Pd, which seems to be consistent in the case of alloy or intermetallic systems reported earlier by us and

other research groups.^{32,34} It should be noted that the spin-orbit splitting value (d) for Cu of both metallic Cu and CuO is ~ 20.2 eV, consistent with the reported results.³⁶ The alloy PdCu/Al₂O₃ catalyst also showed the characteristic satellite peak at 943.8 eV corresponding to Cu(II). These results indicated clearly that metallic Cu, formed upon reduction of the organometallic Cu-salts under the H₂ environment, was involved with the formation of alloy phases between Pd and Cu. In addition to this, CuO was also present with the PdCu/Al₂O₃ catalyst, which was formed most likely by aerial oxidation of the metallic Cu after the synthesis, which is not involved in the alloy formation between Pd and Cu. The amounts of Cu and CuO in the PdCu alloy catalyst were quantified further by integration of individual photo-emission peaks of Cu 2p. It was observed that 58% (~ 0.1527 mmol_{Cu}) and 42% (~ 0.1105 mmol_{CuO}) of Cu and CuO was present in the catalyst, respectively. However, the presence of CuO was not observed in the XRD pattern likely due to the amorphous nature of CuO.

The total amounts of Pd and Cu present in the Pd/Al₂O₃ and PdCu/Al₂O₃ catalysts were quantified by ICP-OES analysis. The estimated amount of Pd present in the Pd/Al₂O₃ and PdCu/Al₂O₃ catalysts is 0.508 and 0.492 mg, respectively, closer to the calculated Pd amounts (5 wt%). Similarly, the amount of Cu present in the alloy PdCu catalyst was estimated to be 0.165 mg, which is again closer to the initially calculated Cu amount (1.67%). It should be noted that both the catalysts were prepared by the deposition of the organometallic Pd- and Cu-salts followed by heating under a H₂ environment at 800 °C and no washing steps were involved in the synthesis of these catalysts. Therefore, it is quite reasonable that the estimated amounts of Pd and Cu present in the catalysts are closer to their initially calculated amounts taken for the synthesis.

Catalytic activity

Catalytic CO oxidation of the Pd/Al₂O₃ and alloy PdCu/Al₂O₃ catalysts is shown in Fig. 5. Both the catalysts showed typical catalytic performance trends, where they didn't show any catalytic activity up to 100 °C, however, they showed significant CO oxidation activity above the temperature of 200 °C. For more details, Pd/Al₂O₃ showed an onset temperature (T_0) (*i.e.*, 1% CO oxidation) at 150 °C and the maximum CO oxidation temperature (T_m) of Pd/Al₂O₃ at 250 °C. Whereas the alloy PdCu/Al₂O₃ catalyst showed improved catalytic CO oxidation activity, where both T_0 and T_m were decreased by 50 °C compared to that of the Pd/Al₂O₃ catalyst. T_0 and T_m of the alloy PdCu/Al₂O₃ catalyst were observed at 100 and 200 °C, respectively. Although the Pd loadings (5 wt%) in both the catalysts are the same, the average particle size of the alloy PdCu nanoparticles is virtually the same as that of the Pd nanoparticles with wide distribution of the PdCu nanoparticles (10–80 nm) compared to that of the Pd nanoparticles (15 and 40 nm); the alloy PdCu/Al₂O₃ catalyst, however, exhibited improved catalytic activity compared with the Pd/Al₂O₃ catalyst due to the alloy structure of PdCu, which has different

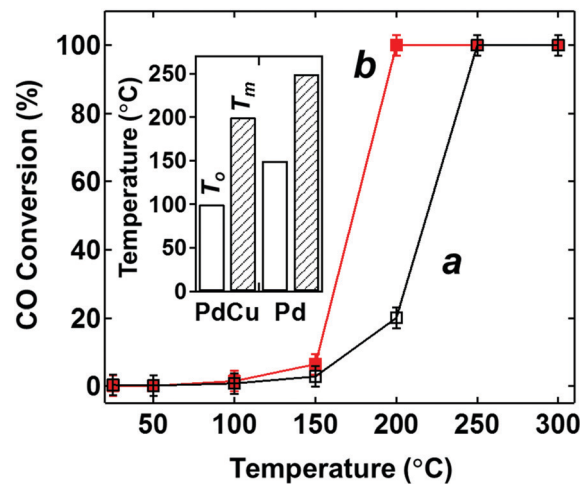


Fig. 5 Catalytic CO oxidation of Pd/Al₂O₃ (a) and alloy PdCu/Al₂O₃ (b) as a function of temperature. Inset shows the comparison of the onset (T_0) and maximum conversion temperature (T_m) of these catalysts.

electronic structure compared with pristine Pd as ensured by the XPS analysis (see Fig. 4 and related discussions). Despite the same Pd-loading and unfavorable particle size and its distribution in the case of the PdCu catalyst compared with the reference Pd catalyst, the electronic structure of the alloy PdCu catalyst may enhance most likely the CO-PROX performance, consistent with the other reported alloy/intermetallic catalysts for several catalysis reactions.^{32,34}

The catalytic CO-PROX performance was also examined further using both the catalysts as shown in Fig. 6. The catalytic CO oxidation in the presence of H₂ is significantly different in particular T_0 compared to that of the catalytic CO oxidation performance in the absence of H₂. It should be noted that both the catalysts showed solely less than 50% activity up to 300 °C in the presence of H₂, whereas they showed 100% CO oxidation catalytic activity at temperatures above 200 °C in the absence of H₂ (see Fig. 5). For more details, Pd/Al₂O₃ showed virtually no CO oxidation in the presence of H₂ up to 150 °C. Whereas the alloy PdCu/Al₂O₃ catalyst showed significant CO oxidation activity compared to that of the Pd/Al₂O₃ catalyst. T_0 of the alloy PdCu and Pd catalysts is 50 and 150 °C, respectively, as shown in Fig. 6 (inset). Interestingly, T_0 of the alloy PdCu/Al₂O₃ catalyst is improved for the CO oxidation in the presence of H₂ compared with the CO oxidation performance in the absence of H₂. The improved CO-PROX catalytic activity of the PdCu catalyst which showed lower onset temperature compared with that of the Pd catalyst is due to the presence of a H₂ rich environment (*i.e.*, reduction environment) that can aid retention of the catalyst in the form of metallic state under CO-PROX conditions. In addition, T_m of both Pd/Al₂O₃ and alloy PdCu/Al₂O₃ catalysts is significantly reduced in the presence of H₂ which was limited to $\sim 45\%$. Both the catalysts showed no significant difference in the CO oxidation performance between 250 and 300 °C in the presence of H₂. It should be noted that both the catalysts showed no significant H₂ conversion up to 300 °C, which is one of the essential prerequisites for the CO-PROX

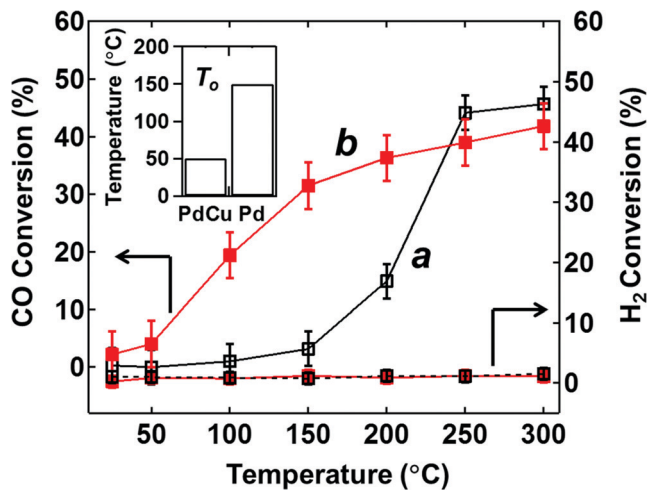


Fig. 6 Catalytic CO oxidation in the presence of H₂ of Pd/Al₂O₃ (a) and alloy PdCu/Al₂O₃ (b) as a function of temperature. H₂ conversion of these catalysts is shown as dotted lines. Inset shows the comparison of the onset (T_o) temperature of these catalysts.

catalyst. However, Pt-based catalysts showed more than 85% superior CO-PROX performance ($T_o = 50$ °C, $T_m = 150$ °C) as reported earlier, compared with the tested Pd-based catalysts in this study.¹⁴ It is worth mentioning here that the selected catalyst is a state-of-the-art Pt-free catalyst and realization of an alloy structure between Pd and Cu can enhance the CO-PROX performance compared with its counterpart Pd catalyst. It is anticipated that reduction in the size of PdCu alloy nanoparticles (average particle size: 30 nm) can improve the CO-PROX performance further, where the size of the state-of-the-art Pt catalytic centres is generally lesser than 5 nm.¹⁴

Selectivity towards the formation of CO₂ without altering the concentration of H₂ during the CO-PROX reaction is another important criterion for the CO-PROX catalysts. Therefore, both the inlet- and outlet-gases were carefully examined further during the CO-PROX reaction. The inlet reactant gases (CO, H₂ and O₂) and CO₂ and the other possible products (*e.g.*, CH₄) due to the undesired reactions from the outlet of the reactor after the CO-PROX reaction were carefully monitored in order to understand the selectivity of the catalysts. As explained, both the catalysts showed selective CO oxidation without changing the H₂ concentration up to 300 °C (inset). Although the catalytic CO oxidation performance of these catalysts increased with increasing temperature under the CO-PROX conditions, it was observed that CH₄ formed above 300 °C was steeply increased with increasing temperature, and reached almost 100% at the temperature of 500 °C as shown in Fig. 7. It should be noted that the conversion of H₂ also increased with increasing the temperature above 350 °C as shown in Fig. 7 (inset). These results implied that the alloy PdCu/Al₂O₃ catalyst can oxidize CO selectively in the presence of H₂ without influencing the H₂ concentration up to the temperature range of 300 °C.

The PdCu catalyst was tested structurally further to examine its stability. It should be noted that the alloy phase of the PdCu catalyst is retained when it was exposed under the harsh

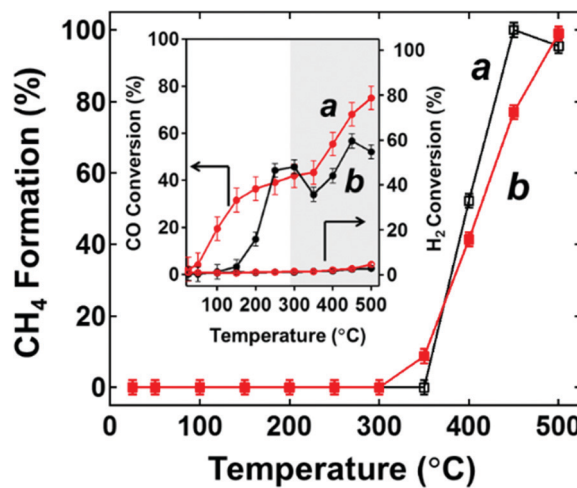


Fig. 7 CH₄ formation as a function of temperature during catalytic CO oxidation in the presence of H₂ of Pd/Al₂O₃ (a) and alloy PdCu/Al₂O₃ (b). The inset shows CO and H₂ conversion of both the catalysts as a function of temperature.

CO-PROX conditions up to 500 °C. Although the intensities of the characteristic diffraction peaks of the PdCu alloy were decreased, their peak positions were not altered significantly (Fig. S2, ESI†). These results implied that the alloy phase between Pd and Cu is stable even after the harsh CO-PROX reactions, which can facilitate the catalytic CO-PROX performance.

Conclusions

Al₂O₃-supported alloy PdCu nanoparticles were synthesized by impregnation of the organometallic Pd- and Cu-salts followed by thermal reduction under a H₂ atmosphere. A higher diffraction shift was observed in the case of alloy PdCu catalysts due to the formation of alloy structures of PdCu. The alloy PdCu nanoparticles are in a spherical shape with an average particle size of 30 nm. The electronic structure of Pd in the alloy PdCu catalysts was altered significantly as its 3d photoemission peak was shifted to a higher binding energy compared to that of the pure Pd catalyst. The Pd-loading of both alloy PdCu and Pd catalysts was the same, which was estimated to be 5 wt.%, however, the alloy PdCu catalyst showed much improved CO oxidation performance compared to that of the reference Pd catalyst both in the presence and absence of H₂. Realization of the Pd-based alloy catalyst structures using copper may have the potential for various catalysis-related applications.

Conflicts of interest

There are no conflicts to declare.

Acknowledgements

The authors gratefully thank the Science and Engineering Research Board (SERB), Department of Science & Technology,

Govt. of India for financial support (EMR/2016/006063). The authors thank the Director, CSIR-NEERI for the guidance and laboratory support of this project. KRC No.: CSIR-NEERI/KRC/2020/MAY/CZC-ERMD/1.

References

- 1 R. Heck and R. Farrauto, *Appl. Catal., A*, 2001, **221**, 443–457.
- 2 S. Rauch, H. F. Hemond, C. Barbante, M. Owari, G. M. Morrison, B. Peucker-Ehrenbrink and U. Wass, *Environ. Sci.*, 2005, **39**, 8156–8162.
- 3 B. A. Gordon, R. Mackay and E. Rehfuss, Health Organization, 2004, <http://www.who.int/iris/handle/10665/42938>.
- 4 M. L. V. Riosa, A. M. Gonzálezb, E. E. S. Lorab and O. A. A. d Olmo, *Biomass Bioenergy*, 2018, **108**, 345–370.
- 5 G. Grzybek, K. Ciura, J. Gryboś, P. Indyka, A. Davó-Quiñonero, D. Lozano-Castelló, A. Bueno-Lopez, A. Kotarba and Z. Sojka, *J. Phys. Chem. C*, 2019, **123**, 20221–20232.
- 6 E. D. Park, D. Lee and H. C. Lee, *Catal. Today*, 2009, **139**, 280–290.
- 7 A. Elmhamdi, L. Pascual, K. Nahdi and A. Martínez-Arias, *Appl. Catal., B*, 2017, **217**, 1–11.
- 8 B. Qiao, J. Liu, Y. Wang, Q. Lin, X. Liu, A. Wang, J. Li, T. Zhang and J. Liu, *ACS Catal.*, 2015, **5**, 6249–6254.
- 9 K. Liu, A. Wang and T. Zhang, *ACS Catal.*, 2012, **2**, 1165–1178.
- 10 A. Fukuoka, J. Kimura, T. Oshio, Y. Sakamoto and M. Ichikawa, *J. Am. Chem. Soc.*, 2007, **129**, 10120–10125.
- 11 V. Ramaswamy, S. Malwadkar and S. Chilukuri, *Appl. Catal., B*, 2008, **84**(1–2), 21–29.
- 12 P. T. A. Santos, A. C. F. M. Costa, R. H. G. A. Kiminami, H. M. C. Andrade, H. L. Lira and L. Gama, *J. Alloys Compd.*, 2009, **483**(1–2), 399–401.
- 13 S. S. Maluf and E. M. Assaf, *Catal. Commun.*, 2011, **12**(8), 703–706.
- 14 R. Khobragade, D. Yearwar, N. Labhsetwar and G. Saravanan, *Int. J. Hydrogen Energy*, 2019, **44**(54), 28757–28768.
- 15 H. Abe, H. Yoshikawa, N. Umezawa, Y. Xu, G. Saravanan, G. V. Ramesh, T. Tanabe, R. Kodiyath, S. Ueda, N. Sekido, Y. Yamabe-Mitarai, M. Shimoda, T. Ohno, F. Matsumoto and T. Komatsu, *Phys. Chem. Chem. Phys.*, 2015, **17**, 4879–4887.
- 16 J. Greeley, I. E. L. Stephens, A. S. Bondarenko, T. P. Johansson, H. A. Hansen, T. F. Jaramillo, J. Rossmeisl, I. Chorkendorff and J. K. Nørskov, *Nat. Chem.*, 2009, **1**, 552–556.
- 17 F. Gao and D. W. Goodman, *Chem. Soc. Rev.*, 2012, **41**, 8009–8020.
- 18 B. Wanjala, R. Loukrakpam, J. Luo, P. Njoki, D. Mott and C. Zhong, *J. Phys. Chem. C*, 2010, **114**, 17580–17590.
- 19 G. Saravanan, K. Pulleri, D. Yearwar, P. Mungse and N. Labhsetwar, *Intermetallics*, 2018, **94**, 179–185.
- 20 D. Wang, H. L. Xin, R. Hovden, H. Wang, Y. Yu, D. A. Muller, F. J. DiSalvo and H. D. Abruña, *Nat. Mater.*, 2013, **12**, 81–87.
- 21 E. Antolini, *Appl. Catal., B*, 2017, **217**, 201–213.
- 22 C. Cui, L. Gan, M. Heggen, S. Rudi and P. Strasser, *Nat. Mater.*, 2013, **12**, 20.
- 23 O. Pozdnyakova, D. Teschner, A. Wootsch, J. Kröhnert, B. Steinhauer, H. Sauer, L. Toth, F. C. Jentoft, A. Knop-Gericke, Z. Paál and R. Schlögl, *J. Catal.*, 2006, **237**, 1–16.
- 24 M. Watanabe, H. Uchida, K. Ohkubo and H. Igarashi, *Appl. Catal., B*, 2003, **46**, 595–600.
- 25 K. Tanaka, Y. Moro-okab, K. Ishigurea, T. Yajimaa, Y. Okabe, Y. Kato, H. Hamanoa, S. Sekiyaa, H. Tanakaa, Y. Matsumotoc, H. Koinumad, H. Hee, C. Zhange and Q. Feng, *Catal. Lett.*, 2004, **92**, 115–121.
- 26 Y. Fan, Y. Zhang, H. Li, W. Shen, J. Wang and M. Wei, *RSC Adv.*, 2016, **6**, 43980–43984.
- 27 P. Mierczynski, K. Vasilev, A. Mierczynska, W. Maniukiewicz and T. P. Maniecki, *Appl. Catal., A*, 2014, **479**, 26–34.
- 28 L. Liu, F. Fan, Z. Jiang, X. Gao, J. Wei and T. Fang, *J. Phys. Chem. C*, 2017, **121**, 26287–26299.
- 29 S. Furukawa, Y. Yoshida and T. Komatsu, *ACS Catal.*, 2014, **4**, 1441–1450.
- 30 M. Armbruster, K. Kovnir, M. Behrens, D. Teschner, Y. Grin and R. Schlogl, *J. Am. Chem. Soc.*, 2010, **132**, 14745–14747.
- 31 X. Nie, X. Jiang, H. Wang, W. Luo, M. J. Janik, Y. Chen, X. Guo and C. Song, *ACS Catal.*, 2018, **8**, 4873–4892.
- 32 L. Di, W. Xu, Z. Zhan and X. Zhang, *RSC Adv.*, 2015, **5**, 71854–71858.
- 33 G. Saravanan, H. Abe, Y. Xu, N. Sekido, H. Hirata, S. Matsumoto, H. Yoshikawa and Y. Yamabe-Mitarai, *Langmuir*, 2010, **26**, 11446–11451.
- 34 T. Gunji, G. Saravanan, T. Tanabe, T. Tsuda, M. Miyauchi, G. Kobayashi, H. Abe and F. Matsumoto, *Catal. Sci. Technol.*, 2014, **4**, 1436–1445.
- 35 J. Batista, A. Pintar, D. Mandrino, M. Jenko and V. Martin, *Appl. Catal., A*, 2001, **206**, 113–124.
- 36 N. Pauly, S. Tougaard and F. Yubero, *Surf. Sci.*, 2014, **620**, 17–22.